Journal of Sound and Vibration (2002) **255**(2), 323–335
doi:10.1006/jsvi.2001.4157, available online at http://www.idealibrary.com on IDEAL®

DISCRETE HUYGENS' MODELLING APPROACH TO WAVE PROPAGATIONS IN A HOMOGENEOUS ELASTIC FIELD

Y. KAGAWA, T. FUJITANI†, Y. FUJITA‡, L. CHAI§, N. WAKATSUKI AND T. TSUCHIYA

Department of Electronics and Information Systems, Faculty of Systems Science and Technology, Akita Prefectural University, 84-4 *Tsuchiya-Ebinokuchi, Honjo city, Akita* 015-0055, *Japan.*
E-mail: y.kagawa@akita-pu.ac.jp

(*Received* 14 *March* 2001, *and in final form* 1 *October* 2001)

The application of the discrete Huygens' modelling has been discussed for acoustic wave propagation problems, in which the scalar wave field problems have been focused. The present paper extends the application of the modelling to the elastic wave propagation in a homogeneous elastic medium in which two types of waves, the longitudinal wave and the shear wave, are independent except at the boundary. Each wave can be treated like a scalar wave until the two waves reach the boundary where they couple so as to satisfy the displacement or stress boundary condition. We propose the approach confining ourselves to the two-dimensional field. Some examples are demonstrated, whose solutions are compared with the vectorial wave modelling and finite difference modelling solutions whenever they are available.

1. INTRODUCTION

This paper is in a series of the discrete Huygens' modelling applied to acoustic problems [1–3]. The discrete Huygens' modelling provides a physical model in which the propagation process is directly traced following the mechanism Huygens explained for the propagation of light. The process of the transmission and scattering is easily implemented on computer in which the wave equation is not numerically solved. It can be proved that the difference equation corresponding to the differential wave equation is derived from the transmission and scattering process [3].

The discrete Huygens' modelling is a synonym of the transmission-line matrix modelling (TLM), which has been extensively used for the electromagnetic wave propagation problems [4–6]. In the present paper, the discrete Huygens' modelling is applied to the wave propagation in a homogeneous elastic medium in two dimensions (x, z co-ordinates). The stress wave field is expressed by the wave equations for two displacement components u_x and u_z. This problem has been considered by Langley *et al.* [7], who developed a complex vectorial element to incorporate the situation. In the present paper, we show that the use of the simple elements for scalar waves as we have discussed for acoustic waves in view of the

†Present affiliation: Kobe Steel Co. Ltd.
‡Present affiliation: Mitsubishi Electric Co. Ltd.
§Present affiliation: Okayama University Graduate School.

0022-460X/02/$35.00

fact that two types of waves, the longitudinal wave and the shear wave, can independently exist until they reach the boundary.

We experience in earthquake that a primary wave comes first and then comes the secondary wave. This is exactly so for the waves in a homogeneous elastic medium, in which the field can be expressed in terms of P and SV waves. Each wave can be treated like a scalar wave to which the algorithm we have developed for the sound wave propagation can directly be applied. The two waves couple only at the field boundary so as to satisfy the displacement or stress boundary condition.

Some simple examples are considered to demonstrate the present technique in which the solutions are compared with those of the other approaches such as the finite difference and the vectorial TLM approach.

2. EQUATIONS OF MOTION FOR ELASTIC WAVES

In the treatment to follow we confine ourselves to the two-dimensional x–z field, in which the phenomena are independent of y direction. The wave equations are given for displacements u_x and u_z as

$$\begin{aligned} \frac{\rho}{\mu}\frac{\partial^2 u_x}{\partial t^2} &= \left(2+\frac{\lambda}{\mu}\right)\frac{\partial^2 u_x}{\partial x^2}+\frac{\partial^2 u_x}{\partial z^2}+\left(1+\frac{\lambda}{\mu}\right)\frac{\partial^2 u_z}{\partial x \partial z}, \\ \frac{\rho}{\mu}\frac{\partial^2 u_z}{\partial t^2} &= \frac{\partial^2 u_z}{\partial x^2}+\left(2+\frac{\lambda}{\mu}\right)\frac{\partial^2 u_z}{\partial z^2}+\left(1+\frac{\lambda}{\mu}\right)\frac{\partial^2 u_x}{\partial x \partial z}, \end{aligned} \tag{1}$$

where ρ is the mass density of the medium, and μ and λ are Lamè's constants. The displacements u_x and u_z are expressed in terms of the two displacement potentials Φ and Ψ defined as

$$u_x = \frac{\partial \Phi}{\partial x}-\frac{\partial \Psi}{\partial z}, \qquad u_z = \frac{\partial \Phi}{\partial z}+\frac{\partial \Psi}{\partial x}. \tag{2}$$

Substitution into equations (1) gives the two expressions

$$\frac{\partial^2 \Phi}{\partial x^2}+\frac{\partial^2 \Phi}{\partial z^2} = \frac{1}{c_p^2}\frac{\partial^2 \Phi}{\partial t^2} \quad \text{for P wave,} \tag{3}$$

$$\frac{\partial^2 \Psi}{\partial x^2}+\frac{\partial^2 \Psi}{\partial z^2} = \frac{1}{c_s^2}\frac{\partial^2 \Psi}{\partial t^2} \quad \text{for SV wave.} \tag{4}$$

The wave equations are now independent for Φ and Ψ, respectively, and the propagation velocities are given by

$$c_p = \sqrt{\frac{\lambda+2\mu}{\rho}} = \sqrt{\frac{E}{\rho}}\sqrt{\frac{1-\sigma}{(1+\sigma)(1-2\sigma)}} \quad \text{for P wave,} \tag{5}$$

$$c_s = \sqrt{\frac{\mu}{\rho}} = \sqrt{\frac{E}{\rho}}\sqrt{\frac{1}{2(1+\sigma)}} \quad \text{for SV wave,} \tag{6}$$

where E and σ are Young's modulus and Poisson's ratio. The P wave travels faster than the SV wave. The velocity ratio is

$$\frac{c_s}{c_p} = \sqrt{\frac{1-2\sigma}{2(1-\sigma)}}. \tag{7}$$

3. DISCRETE HUYGENS' MODEL

3.1. ELEMENT

Equations (3) and (4) are the wave equations for the P and SV waves. Each of them is expressed in terms of a potential wave. The scalar wave modelling which we presented in our previous papers could be used [3]. Now the field is modelled by independent two-layered networks, as shown in Figure 1, in which each consists of a series of the connection of the elements with four and five branches. An element for the P wave is shown in Figure 2 in which the scattering of the impulses are also shown. The scattering matrix is given by

$$\begin{bmatrix} \Phi_1 \\ \Phi_2 \\ \Phi_3 \\ \Phi_4 \end{bmatrix}^r = \frac{1}{2} \begin{bmatrix} -1 & 1 & 1 & 1 \\ 1 & -1 & 1 & 1 \\ 1 & 1 & -1 & 1 \\ 1 & 1 & 1 & -1 \end{bmatrix} \begin{bmatrix} \Phi_1 \\ \Phi_2 \\ \Phi_3 \\ \Phi_4 \end{bmatrix}^i. \tag{8}$$

The relation between the incident and reflected impulses about the node is defined by

$$\Phi = \sum_{n=1}^{4} (1+s)\Phi_n^i = \frac{1}{2}\sum_{n=1}^{4} \Phi_n^i, \qquad \Phi_n^r = \Phi - \Phi_n^i, \tag{9}$$

where Φ is the potential in the P wave network, Φ_n^i and Φ_n^r are incident and reflected impulses at branch n ($n = 1$–4) of the element, and s is the reflection coefficient at the node

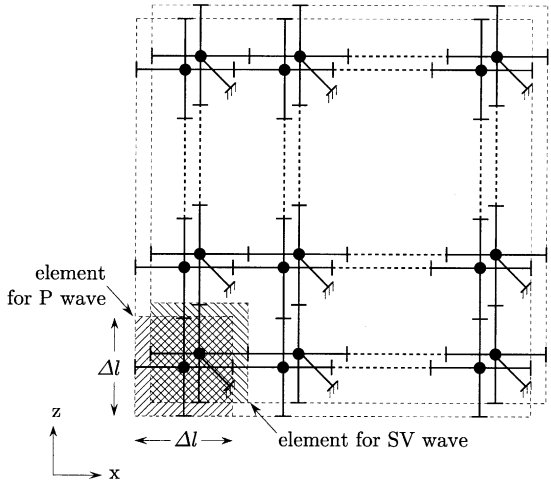

Figure 1. Two-layered network for two potential waves.

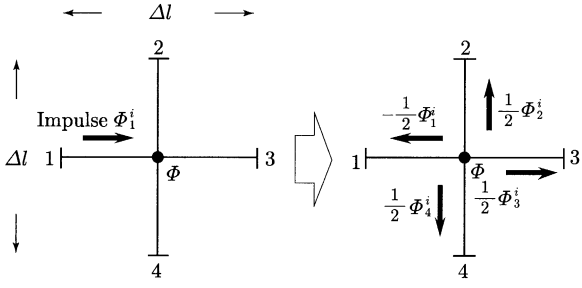

Figure 2. Scattering of impulses at the element node (P wave).

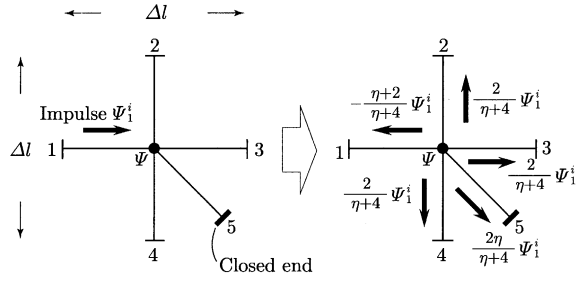

Figure 3. Element for SV wave and scattering of impulses at the node (SV wave).

defined by

$$s = \frac{Z_0/3 - Z_0}{Z_0/3 + Z_0} = -\frac{1}{2}, \tag{10}$$

where Z_0 is the characteristic impedance of the branch.

It should be noted that the propagation velocity in the network $\bar{c}_p$ is slower than that in the free medium c_p by a factor of $1/\sqrt{2}$ ($\bar{c}_p = c_p/\sqrt{2}$).

A similar modelling is possible for the wave equation (4) of the SV wave, which propagates slower than the longitudinal wave. A delay mechanism can be devised for the element without violating the temporal synchronization. It is made simply by providing a fifth branch as shown in Figure 3. η is the parameter which makes the propagation speed slower. The scattering matrix is given by

$$\begin{bmatrix} \Psi_1 \\ \Psi_2 \\ \Psi_3 \\ \Psi_4 \\ \Psi_5 \end{bmatrix}^r = \frac{1}{\eta+4} \begin{bmatrix} -(\eta+2) & 2 & 2 & 2 & 2\eta \\ 2 & -(\eta+2) & 2 & 2 & 2\eta \\ 2 & 2 & -(\eta+2) & 2 & 2\eta \\ 2 & 2 & 2 & -(\eta+2) & 2\eta \\ 2 & 2 & 2 & 2 & \eta-4 \end{bmatrix} \begin{bmatrix} \Psi_1 \\ \Psi_2 \\ \Psi_3 \\ \Psi_4 \\ \Psi_5 \end{bmatrix}^i. \tag{11}$$

The relation between the impulses about the node is defined by

$$\Psi = \frac{2}{\eta+4} \sum_{n=1}^{4} \Psi_n^i + \frac{2\eta}{\eta+4} \Psi_5^i, \qquad \Psi_n^r = \Psi - \Psi_n^i \quad (n = 1\text{–}5), \tag{12}$$

where Ψ is the potential in the SV wave network, Ψ_n^i is the in-coming impulse to the corresponding branch n and Ψ_n^r is the reflected impulse from the node to the corresponding branch. The end of the fifth branch is closed, so that $\Psi_5^i = \Psi_5^r$.

3.2. ELEMENT CONNECTION

Each wave field consists of a network of the elements connected in both x and z directions, over which impulses advance the distance Δl for the duration Δt or at the speed $\Delta l/\Delta t$. The branch 1 of an element is connected to the branch 3 of another adjacent element and so on, in which the incident impulses to the node (x_p, z_q) at the time t_k correspond to the reflected impulses scattered from the surrounding elements at the previous time t_{k-1}. The subscript k indicates the number of the steps corresponding to the time $k\Delta t$.

One has the compatibility for the connection

$$\begin{aligned}
{}_k\Phi_1^i(x_p, z_q) &= {}_{k-1}\Phi_3^r(x_{p-1}, z_q),\\
{}_k\Phi_2^i(x_p, z_q) &= {}_{k-1}\Phi_4^r(x_p, z_{q+1}),\\
{}_k\Phi_3^i(x_p, z_q) &= {}_{k-1}\Phi_1^r(x_{p+1}, z_q),\\
{}_k\Phi_4^i(x_p, z_q) &= {}_{k-1}\Phi_2^r(x_p, z_{q-1}).
\end{aligned} \tag{13}$$

This relation holds for every element over P wave network, which together with the scattering algorithm (9) establishes the wave propagation. Similar expression is also valid for the SV wave, expect the presence of the fifth branches with their other ends closed. Subscripts p and q refer to the position of the element in x and z co-ordinates.

If the displacement solutions are required, they are obtained from the finite difference calculation of

$$\begin{aligned}
u_x &= \frac{1}{2\Delta l}\left[\{\Phi(x_{p+1}, z_q) - \Phi(x_{p-1}, z_q)\} - \{\Psi(x_p, z_{q+1}) - \Psi(x_p, z_{q-1})\}\right],\\
u_z &= \frac{1}{2\Delta l}\left[\{\Phi(x_p, z_{q+1}) - \Phi(x_p, z_{q-1})\} + \{\Psi(x_{p+1}, z_q) - \Psi(x_{p-1}, z_q)\}\right].
\end{aligned} \tag{14}$$

4. BOUNDARY CONDITIONS

There are three typical boundaries to be encountered in the practical situations, which are the non-reflective or absorbing boundary, the fixed boundary and the free boundary. Here only first two cases are considered, as demonstrated in reference [7], in which a vectorial element is developed for the elastic waves.

4.1. NON-REFLECTIVE BOUNDARY

Non-reflective boundary is the boundary at which the waves coming into the boundary is absorbed. This condition can be realized simply by terminating the boundary with the

characteristic impedance at the end of the corresponding branches of the elements attached to the boundary. The termination can independently be made for the P wave and the SV wave, respectively, without coupling.

4.2. FIXED BOUNDARY

The displacements are fixed so the $u_x = u_z = 0$ on the boundary. In our present modelling, the condition must be prescribed in terms of the displacement potentials. The finite difference expressions of equation (14) must be zero at all times. That is

$$u_x(x_p, z_q) = 0, \quad u_z(x_p, z_q) = 0, \tag{15}$$

which are applied to the elements attached to the boundary. When the boundary is set parallel to the x-axis at $z = z_p$ as shown in Figure 4, Φ_2^i and Ψ_2^i are out of the region and unknown. Solving equations (14) for $\Phi(x_{p+1}, z_q)$ and $\Phi(x_{p+1}, z_q)$, gives

$$\begin{aligned} \Phi(x_p, z_{q+1}) &= \Phi(x_p, z_{q-1}) + \Psi(x_{p+1}, z_q) - \Psi(x_{p-1}, z_q), \\ \Psi(x_p, z_{q+1}) &= \Psi(x_p, z_{q-1}) + \Phi(x_{p+1}, z_q) - \Phi(x_{p-1}, z_q). \end{aligned} \tag{15'}$$

With the help of equations (9) and (13), the impulses arriving to the node (x_p, z_q) from the outer region are obtained for each element, which are

$$\begin{aligned} {}_{k+1}\Phi_2^i(x_p, z_q) &= {}_k\Phi_4^r(x_p, z_{q+1}) \\ &= {}_k\Phi(x_p, z_{q+1}) - {}_k\Phi_4^i(x_p, z_{q+1}), \\ {}_{k+1}\Psi_2^i(x_p, z_q) &= {}_k\Psi_4^r(x_p, z_{q+1}) \\ &= {}_k\Psi(x_p, z_{q+1}) - {}_k\Psi_4^i(x_p, z_{q+1}). \end{aligned} \tag{16}$$

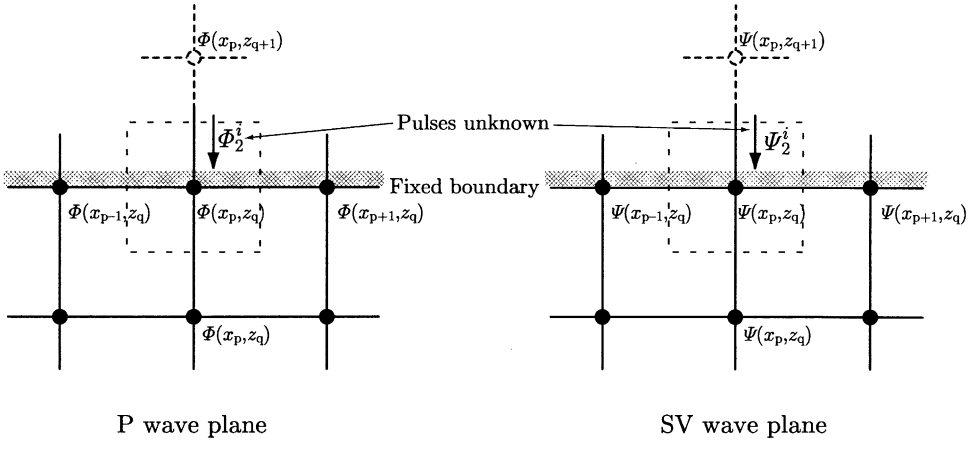

Figure 4. Impulse transition over the fixed boundary.

The right side are all the arriving impulses. Additional computation is required for processing the boundary conditions.

5. VECTORIAL WAVE APPROACH MODELLING

A scalar wave approach is possible for each wave so that the discrete Huygens' modelling developed in our previous papers can directly be applied at the expense of the additional processing cost for the boundary. In the preceding sections, we presented how to incorporate the coupling of the P and SV waves at the boundaries. Langley *et al.* [7] developed an eight-branches element for modelling the vectorial wave propagation in the two-dimensional elastic medium, in which the formulation is made directly for the displacements. The modelling is very complicated though it could be applied to the non-homogeneous elastic field. The scattering matrix consists of 8×8 components in which the computation is more expensive, while our present approach requires only two 4×4 matrices with additional computation for processing the boundary conditions.

It should be noted that their modelling is formulated in such a way that the P and SV waves are coupled within an element, while in our present modelling the two waves are independent until they reach the boundary where they couple. In the examples to follow, the simulations are compared with other approaches to demonstrate the validity of our modelling.

6. SOME NUMERICAL VERIFICATIONS

6.1. WAVE PROPAGATION VELOCITY

We take a square field made of $200\Delta l \times 200\Delta l$. The plane wave excitation is made over one of the boundaries of the square field on the left-hand side at which a single shot sine wave with duration $30\Delta t$ is given. Other boundaries are treated to be non-reflective. The Poisson's ratio of the medium is taken to be $\sigma = 0{\cdot}3$. The snap shot waveforms at the position $(50\Delta l, 100\Delta l)$ are shown in Figure 5, in which the results of the FD-TD method using the scalar wave modelling are also shown for the purpose of verification. All three traces agree. The ringing may be the effect due to the higher frequency spectra of the single shot.

The velocity ratio calculated from the time required for the transit of a certain length is $c_s/c_p = 0{\cdot}536$, whose theoretical counterpart is $c_s/c_p = 0{\cdot}5345$. The agreement is reasonable.

6.2. MODE CONVERSION

Here we again consider the square field ($200\Delta l \times 200\Delta l$) in which the three boundaries are non-reflective and the fixed boundary is set on the right side as shown in Figure 6. A single shot sine P wave is excited over the diagonal line. The displacements are depicted in Figure 7 at various time steps, in which only the region corresponding to the shaded area in Figure 6 is shown. The lines indicate the direction and the amplitude by their length. It is seen that on the arrival of the wave front of the P wave to the fixed boundary, the reflection is taken place and the SV wave is simultaneously generated. The amplitude ratios to the reflected waves are

$$\left|\frac{\Phi^r}{\Phi^i}\right| = 0{\cdot}412 \quad (0{\cdot}42) \qquad \left|\frac{\Psi^r}{\Phi^i}\right| = 1{\cdot}082 \quad (1{\cdot}058),$$

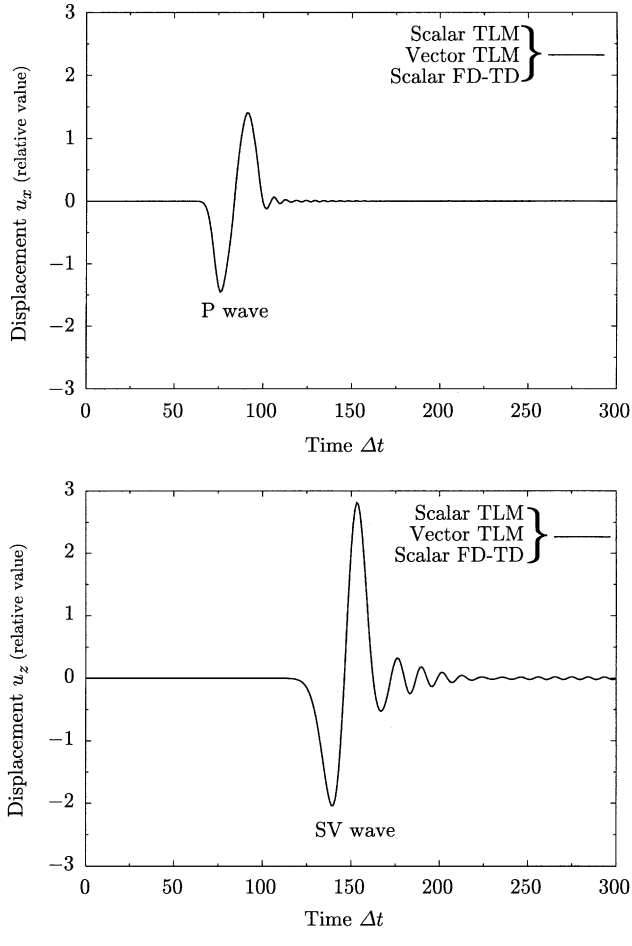

Figure 5. Travelling of a single shot sine wave.

where $|\Phi^i|$ is the amplitude of the incident P wave. $|\Phi^r|$ and $|\Psi^r|$ are the amplitudes of the reflected waves for the P wave and the SV wave respectively. The theoretical values are given in parentheses. The results show the validity of the present approach and modelling.

7. REFLECTIONS AT THE BOUNDARY

7.1. FIXED BOUNDARY

Here we again demonstrate what happens at the fixed boundary. We consider a square field of $200\Delta l \times 200\Delta l$, in which the boundary is fixed at the upper end as shown in Figure 8. A single shot sine wave (both P and SV waves) of duration $300\Delta t$ with a unit amplitude is excited at the point $(101\Delta l, 151\Delta l)$. The process of the propagation is illustrated in Figure 9, in which the displacement distributions at various time steps are shown. The P wave omnidirectionally advances first and then comes the SV wave. When the P wave hit the fixed boundary, the P wave is reflected and the SV wave is generated. When the SV wave

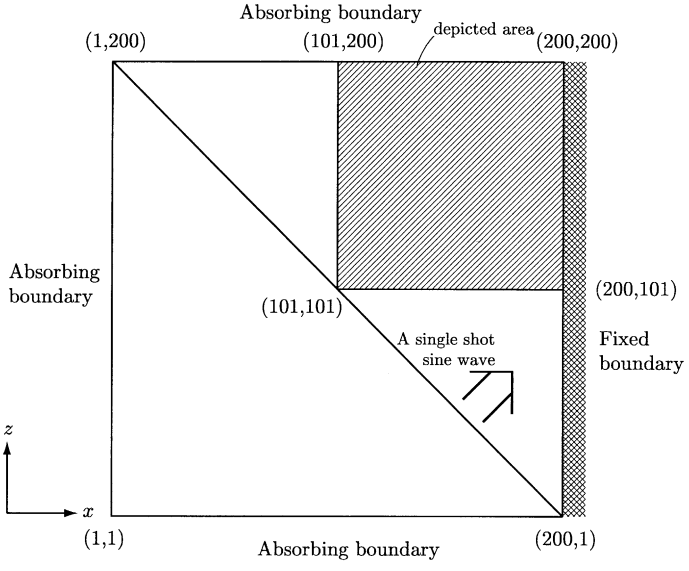

Figure 6. Oblique incident modelling field.

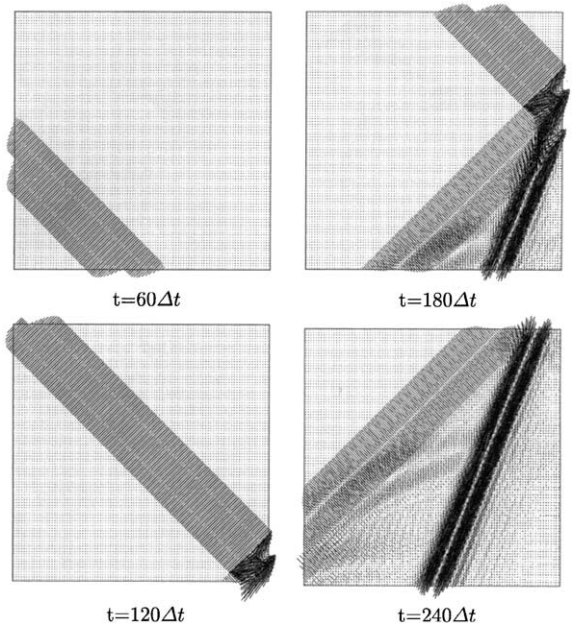

Figure 7. Mode conversion at the fixed boundary.

then hit the boundary, SV wave is reflected with the generation of the P wave. Figure 10 shows the corresponding situation simulated by the vectorial wave modelling [7], in which it is seen that the propagation is also omnidirectional but with somewhat square-like shape. The waveforms obtained at the point ($151\Delta l$, $101\Delta l$) are shown in Figure 11. The ringing is more pronounced in the waveforms based on the vectorial wave modelling.

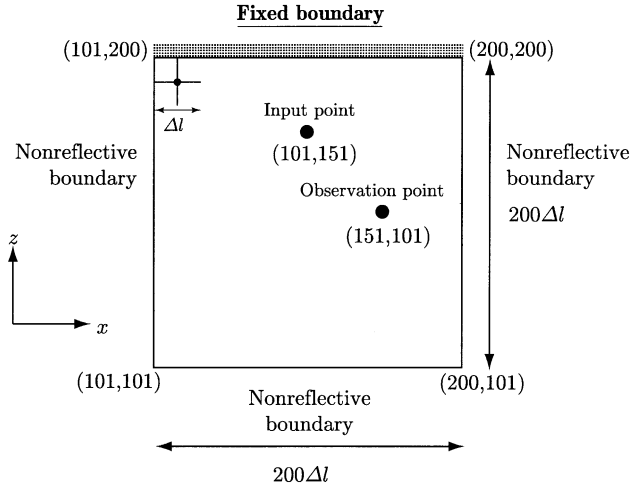

Figure 8. Field with the fixed boundary.

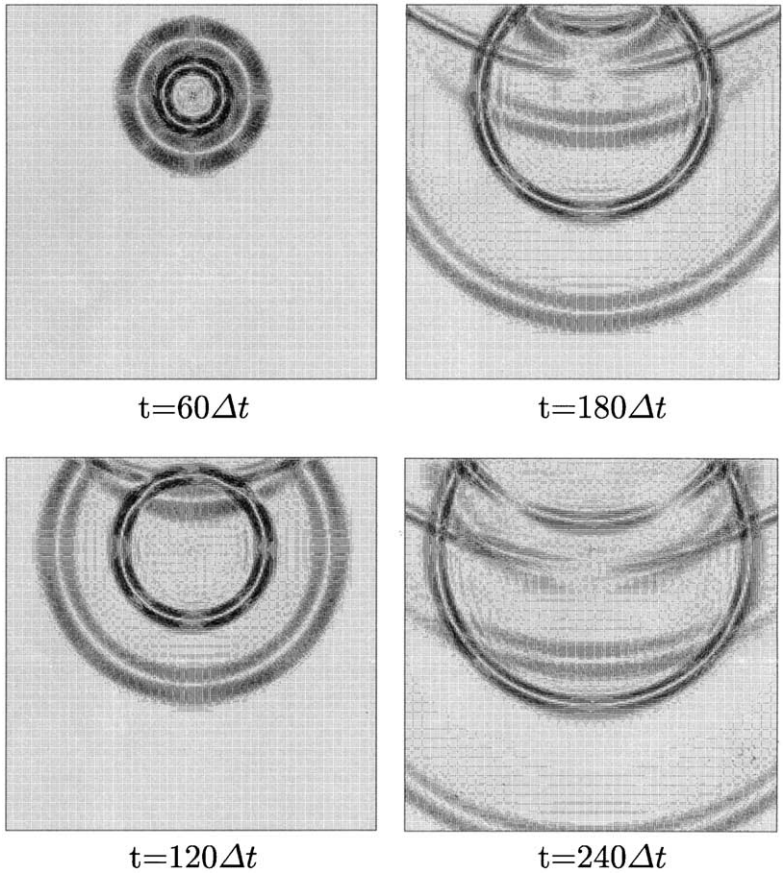

Figure 9. Wave propagation and reflection at the boundary in displacements (scalar wave modelling).

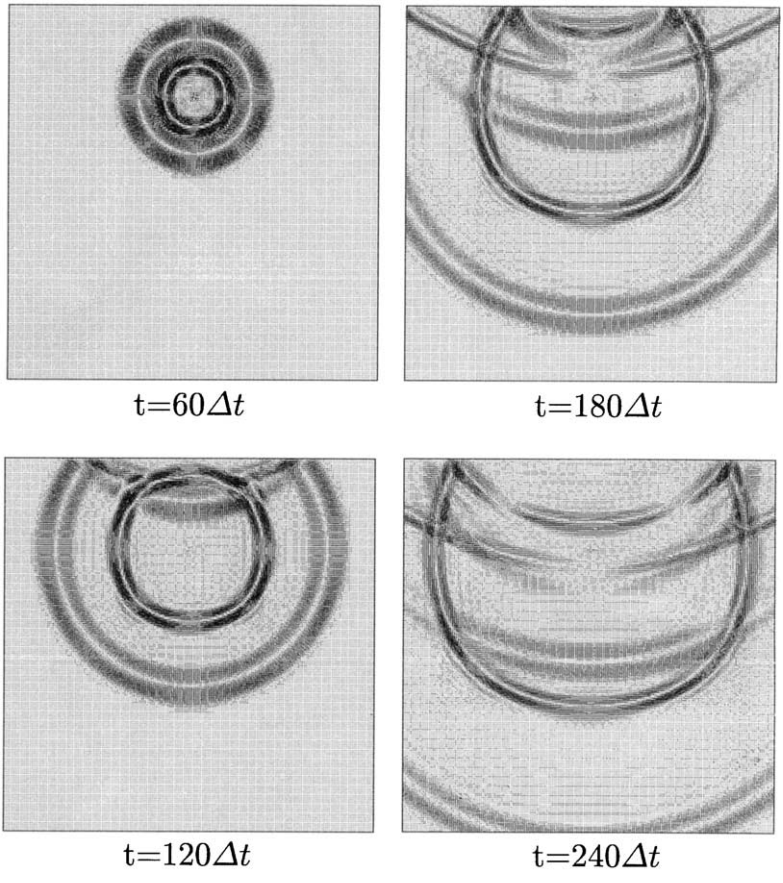

Figure 10. Wave propagation and reflection at the boundary in displacements (vectorial wave modelling).

8. DISCUSSIONS

We have presented that the scalar wave approach is possible with the scalar TLM modelling for the wave propagation in a homogeneous elastic medium. As demonstrated, the scalar wave approach gives more realistic solutions. The approach can contribute to the reduction of the computational resources by about a half with some additional cost for the boundary condition processing. The displacement expressions are not always requested.

Comparison with other numerical methods will be discussed in the following. The most popular numerical approaches to wave propagation problems are the FD-TD and FE methods. As shown previously [1], the order of the errors of the present method is of the same order as that of the FD-TD and FEM with the first order trial function for an element used. In these methods, the space can be discretized independent of the time discretization. Though the discretization is thus chosen independently, a stable time step should be examined. The present method is essentially stable.

In the FD-TD and FEM, a pre-processing stage is required which is to form the system matrix or coefficient matrix for the simultaneous differential equations of the second order with respect to time. They are then to be solved by the time marching method such as Newmark β scheme. In these methods, the computation is global in space in which the solution of the simultaneous equations is required in each time step, while in the present

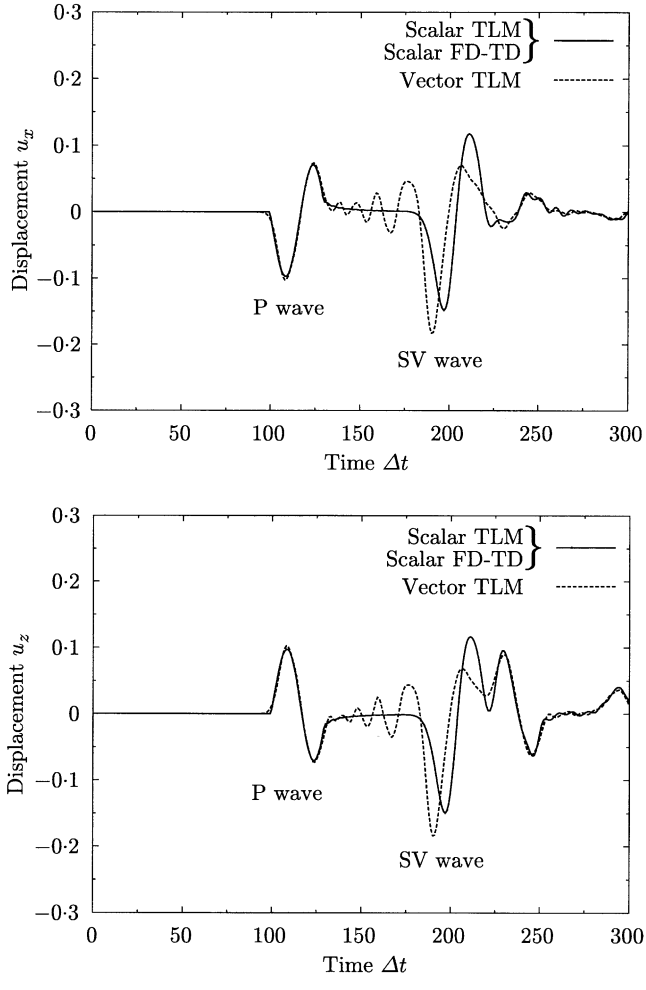

Figure 11. Displacement wave forms observed at ($151\Delta l$, $101\Delta l$).

approach, the computation is local. The number of the operations required for the single step of the computation is thus proportional to N, number of the nodes or the elements in the present approach, while the FD-TD and FEM require the N^2 operations. However, their system matrix is usually banded with the bandwidth W so that the number of the operations is proportional to WN. The solution of the simultaneous equation is also localized. As the bandwidth is about 6 for the square elements, their computational costs will be more than 6 times compared with that of the present method.

9. CONCLUDING REMARKS

The discrete Huygens' modelling approach was extended to the wave propagation in a homogeneous elastic medium. It was shown that the scalar wave approach was possible by the use of the scalar TLM elements, in which the P and SV waves were treated independently until they reached the boundary at which they couple. To show the validity of the modelling and the approach, some numerical demonstrations were presented. The

solutions were verified in comparison with the solutions by the vectorial wave modelling approach and finite difference method. As in reference [7], the case of the free boundary could not be included at the present stage. Both the solutions were found to be unstable.

ACKNOWLEDGMENTS

Acknowledgments go to T. Arima and N. Koyama who are appreciated for their co-operation in the course of the present study.

REFERENCES

1. Y. KAGAWA, T. TSUCHIYA, B. FUJII and K. FUJIOKA 1998 *Journal of Sound and Vibration* **218**, 419–444. Discrete Huygens' model approach to sound wave propagation.
2. Y. KAGAWA, T. TSUCHIYA, K. FUJIOKA and M. TAKEUCHI 1999 *Journal of Sound and Vibration* **225**, 61–78. Discrete Huygens' model approach to sound wave propagation—reverberation in a room, sound source identification and tomography in time reversal.
3. Y. KAGAWA, T. HARA and T. TSUCHIYA 2001 *Journal of Sound and Vibration* **243**, 419–439. The discrete Huygens' modelling in the propagation velocity varying environments.
4. W. J. HOEFER and P. P. M. SO 1991 *The Electromagnetic Wave Simulator*. New York: John Wiley & Sons.
5. C. CHRISTOPOULOS 1995 *The Transmission-line Modelling Method—TLM*. New York: IEEE Press.
6. Y. KAGAWA, N. YOSHIDA, T. TSUCHIYA and M. SATO 2000 *JSST Computational Electromagnetics and Electronics Series* 4. *Introduction to Equivalent Circuit Network Methods—Transmission-Line Modelling Method and Spatial Circuit Network Method*. Tokyo: Morikita Pub. Co.
7. P. LANGLEY, S. H. PULKO and A. J. WILKINSON 1996 *International Journal Numerical Modeling—Electronic Networks, Devices and Fields* **9**, 429–443. A TLM model of transient 2-dimensional stress propagation.